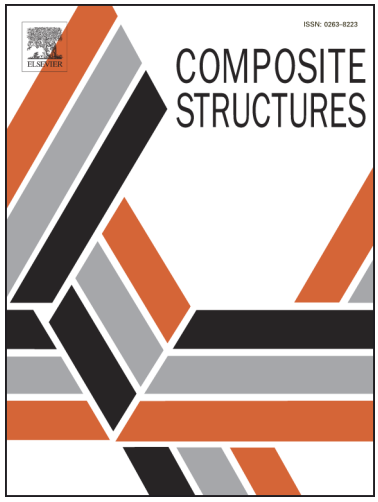

Damage tolerance optimization of composite stringer run-out under tensile load

P. Badalló, D. Trias, E. Lindgaard

PII: S0263-8223(15)00569-3
DOI: http://dx.doi.org/10.1016/j.compstruct.2015.07.025
Reference: COST 6604

To appear in: *Composite Structures*

Received Date: 23 March 2015
Revised Date: 7 July 2015
Accepted Date: 12 July 2015

Please cite this article as: Badalló, P., Trias, D., Lindgaard, E., Damage tolerance optimization of composite stringer run-out under tensile load, *Composite Structures* (2015), doi: http://dx.doi.org/10.1016/j.compstruct.2015.07.025

Damage tolerance optimization of composite stringer run-out under tensile load

P. Badalló[a], D. Trias[a], E. Lindgaard[b]

[a]*AMADE, Dept. of Mechanical Engineering and Industrial Construction, Universitat de Girona, Campus Montilivi s/n, E-17071 Girona, Spain*
[b]*Department of Mechanical and Manufacturing Engineering, Aalborg Universitet, Fibigerstraede 16, DK-9220 Aalborg Øst, Denmark*

Abstract

Stringer run-outs are a common solution to achieve the necessary strength, stiffness and geometric requirements of some structural solutions. The mechanical behaviour and complexity of such design details requires careful and thorough studies to ensure the structural integrity of the structure. The influence of some geometric variables of the run-out in the interface of the set stringer-panel is crucial to avoid the onset and growth of delamination cracks. In this study, a damage tolerant design of a stringer run-out is achieved by a process of design optimization and surrogate modelling techniques. A parametric finite element model created with *python* was used to generate a number of different geometrical designs of the stringer run-out. The relevant information of these models was adjusted using Radial Basis Functions (RBF). Finally, the optimization problem was solved using Quasi-Newton method and Genetic Algorithms. In the solution process, the RBF were used to compute the objective function: ratio between the energy release rate and the critical energy release rate according to the Benzeggagh-Kenane mixed mode criterion. Some design guidelines to obtain a damage tolerant stringer-panel interface have been derived from the results.

Keywords:

Metamodeling, Radial Basis Function, Genetic Algorithm, Fracture Mechanics, Stiffened Panels.

Email addresses: pere.badallo@udg.edu (P. Badalló), dani.trias@udg.edu (D. Trias)

1. Introduction

The benefits of composite materials in aircraft/aerospace structures have been demonstrated in the last years. Stiffened panels are a common design strategy to obtain high stiffness in shell structures, keeping the lightness of the component and ensure the required buckling strength of the shell structure. As many others commonly used structural subcomponents these structures are frequently analysed [1–4] using the so-called virtual tests, which aims to reduce the design cost by reducing the number of test on real components.

One method to increase stiffness and buckling strength of shells is the use of stringers which are efficient but requires careful analysis and design of the panel-stringer interface [5–7]. Additionally, the geometric specification of the design sometimes requires a special termination of the stringer named run-out, which is a cut-out showing a certain angle at the tip. This termination can be classified to different types and geometries. Run-outs have been analysed by different authors [8–12] to define the behaviours and the best design. Hence, virtual tests, sometimes accompanied by experimental tests, have been deeply used to design and help to manufacture composite stringer run-outs [13–17].

However, the use of virtual tests needs large computation time for complex models. This prevents the use of optimization methods due to the necessity of generating a large number of different design cases (geometric, load states, boundary conditions, etc.) and their high computational cost. Metamodeling (or surrogate modeling) methods [18] are approximation techniques which can be used to substitute partially the solution of a complete finite element model. The use of surrogate models for design optimization or control of nonlinear systems has increased significantly in the last decade. The idea of surrogate models is to alleviate the burden of performing many computationally expensive analyses on a detailed model by constructing an approximation model (the surrogate model), that mimics the behaviour of the detailed simulation model as closely as possible while being computationally inexpensive to evaluate. Metamodeling may thus enable the use of design optimization techniques of complex and numerically expensive systems [19, 20].

In the present study, an optimization process with the aim of obtaining a damage tolerant design of run-out has been established and conducted. A parametric virtual test has been developed

(Section 2) and Virtual Crack Closure Technique (VCCT) in the interface panel-stringer has been implemented. The structural influence of the different geometric variables of a run-out have been studied to choose the most significative ones (Section 3.1). The creation and verification of a Radial Basis Function (RBF) to reduce the computational time has been achieved (Section 3.4). Finally, optimizations of the RBF with Quasi-Newton method and Genetic Algorithms (GA) with different variable intervals have been performed and compared (Section 4).

2. Virtual test

2.1. Specimen and test

The study carried out by Greenhalgh and Garcia [11] has been used to design the specimen and virtual test. The specimen is a panel with an attached stringer run-out. This specimen was also used in a previous work [21] by the authors of the present paper to analyse the mechanical response of the different geometries and achieve a better understanding of the component and the test. A displacement boundary condition δ is applied at the tip of the specimen (Fig. 1(a)). The stringer run-out of this model is defined by four variables: the stringer rib angle α, the stringer base angle β, the distance between the rib tip and the stringer base tip d, and the distance between the stringer base and the point where the stringer rib angle starts L_{ro} (Fig. 1(b)). In this study, *python* code together with ABAQUS$^{\text{TM}}$ 6.12-1 Standard [22] have been used to create a parametric model that automatically can be generated.

[Figure 1 about here.]

VCCT is used to determine the energy release rate of the existing initial crack (explained in Section 2.2). Previous work [21] shows that the formation of a crack always appears in the tip of the stringer base. For this reason, the initial crack is modelled in all the different cases at this location, in the longitudinal midplane between the stringer and the panel.

The material for both the stringer and the panel is AS4/8552 and they are bonded using FM-300K adhesive. All the material properties are described in Table 1.

[Table 1 about here.]

2.1.1. Mesh

A comparative analysis was performed to determine the most appropriate element type. The elements compared have been C3D8 (8-node linear brick three-dimensional solid element), C3D8R (8-node linear brick three-dimensional solid element with reduced integration and hourglass control), C3D8I (8-node linear brick three-dimensional solid element with incompatible modes), C3D20 (20-node quadratic brick three-dimensional solid element) and SC8R (8-node, quadrilateral, first-order interpolation, stress/displacement continuum shell element with reduced integration). Solution time, reaction force and out-of-plane displacement have been compared through mesh convergence studies (Table 2). All the element types have been compared with C3D20 element because it is well suited for bending problems. In our case, the computation time of SC8R element model is 100 times faster. The relative error is 0.14% and 1.69% in the reaction force and out-of-plane displacement, respectively. Therefore, SC8R element was chosen to mesh the whole model because it reduces the computational time and obtains reliable results.

[Table 2 about here.]

The model has been partitioned in three parts (Fig. 2) to control all the element sizes of the mesh. These three parts are the stringer (without the crack zone), panel (without the crack zone) and the crack zone. All the parts have been bonded using TIE constraints (Fig. 2). The distance between the crack tip to the TIE zone has been analysed carefully to avoid interferences between the TIE constraint and VCCT (contact constraint in ABAQUS™).

[Figure 2 about here.]

Krueger [23] proposes some guidelines about mesh size for the correct application of the VCCT (Section 2.2) in composite materials. The authors performed a sensitivity analysis concerning the dependence of the total energy release rate ($\mathcal{G}$) on the element length ($\triangle a$). According to Krueger, the element length ($\triangle a$) should be compared with the ply thickness h. A stabilization of the curve $\mathcal{G}$ vs. ${}^{\triangle a}/_{h}$ was achieved for about ${}^{\triangle a}/_{h} = 1$, which meets the upper bound of Krueger's recommendation. Consequently, since $h = 0.18$mm, $\triangle a$ was set to 0.18mm in the crack zone.

In all the designed cases the mesh in the crack zone is controlled. Fig. 2 shows that the mesh in this zone is regular with the needed size to guarantee the correct computation of the VCCT.

2.2. Virtual Crack Closure Technique

VCCT [23] is used to calculate the energy release rate ($\mathcal{G}$). This technique assumes that the crack growth is self-similar. This means that if only the crack tip is observed, in the current step, the crack shape (displacements) and the reaction forces at the crack tip are assumed identical to those at the previous step.

The mixed mode fracture toughness, $\mathcal{G}_{\mathrm{C}}$, has been calculated with the formulation of Benzeggagh-Kenane [24].

$$\mathcal{G}_{\mathrm{C}} = \mathcal{G}_{\mathrm{I_C}} + (\mathcal{G}_{\mathrm{II_C}} - \mathcal{G}_{\mathrm{I_C}}) \cdot B^{\eta} \tag{1}$$

where $\mathcal{G}_{\mathrm{I_C}}$ and $\mathcal{G}_{\mathrm{II_C}}$ are the critical energy release rate in mode I (opening) and mode II (sliding), respectively. η is the Benzeggagh-Kenane interaction parameter between modes and B is the shear mode ratio calculated by:

$$B = \frac{\mathcal{G}_{\mathrm{II}} + \mathcal{G}_{\mathrm{III}}}{\mathcal{G}} \tag{2}$$

where $\mathcal{G}$ is the total energy release rate, calculated as $\mathcal{G}_{\mathrm{I}} + \mathcal{G}_{\mathrm{II}} + \mathcal{G}_{\mathrm{III}}$, and $\mathcal{G}_{\mathrm{I}}$, $\mathcal{G}_{\mathrm{II}}$ and $\mathcal{G}_{\mathrm{III}}$ are fracture energies in mode I, mode II and mode III (tearing), respectively.

3. Optimization

3.1. Design variables

The first model of the stringer run-out was defined with 4 parametric variables (Fig. 1): α, β, d and L_{ro}. In order to know if all these variables have a significant influence in the objective function, the analysis of variance test (ANOVA) [25] was used. The purpose of this test is to determine if the mean values of a group of data are significantly different to the values of another group of data. A group of data is significant when the probability (p-value) is less than a threshold (normally fixed between 0.05 and 0.01).

In our case, a group of 150 different design cases has been used to apply the ANOVA test. The results obtained are described in Table 3.

[Table 3 about here.]

The obtained results (Table 3) indicate that α and L_{ro} are not significant for the value of the objective function. For this reason, only β and d have been selected as design variables for the optimization problem. The p-value computed for d is slightly greater than the threshold normally accepted. However, this value is significantly lower compared with α and L_{ro} . For this reason, d is accepted like an influential variable on the objective function.

3.2. Optimization problem

It is nowadays well-known that damage tolerant design in brittle and quasi-brittle materials like CFRP has to be based on fracture mechanical analysis, instead of using stress based criteria because of the difficulty of computing the stress field closes to the singularity (brittle materials) and at the failure process zone (quasi-brittle materials) [26]. For this reason, when looking for an optimal design in terms of damage tolerance, the objective function has to include some measure of the capacity of a crack to grow under the specified load. The failure index (Eq. 3) used as objective function in this study includes the current energy release rate normalized to the current critical energy release rate both depending on the current mode-mixity.

$$FI = \frac{\mathcal{G}}{\mathcal{G}_{\text{C}}} \tag{3}$$

The objective of the optimization problem is to minimize the FI, that is $FI(\beta, d)$. Stringer base angle β and the distance d between the rib tip and the stringer base tip are the two design variables, so the optimization problem is defined as:

$$\begin{aligned} &\text{Minimize} && FI(\beta, d) \\ &\text{Subject to} && 0 \leq \beta \leq 60 \\ & && 0 \leq d \leq 47 \end{aligned} \tag{4}$$

A Quasi-Newton method and a Genetic Algorithm (GA) [27] have been used to carry out the optimization. Quasi-Newton method is implemented in the function *fmincon* of the Optimization Toolbox™ of the commercial software MATLAB® [28]. A Non-dominate Sorting Genetic Algorithm II (NSGA-II) [29] is the variant used to achieve the optimization (implemented in the Optimization Toolbox™ of MATLAB®). In a previous work [30] NSGA-II was determined as one of the most effective algorithms.

3.3. Data sampling

The use of adequate "training" sample is crucial to obtain acceptable accuracy of the RBF (Section 3.4). For this reason, the correct distribution of the analysed cases has to be considered. In this study a Latin Hypercube Sampling (LHS) [31] has been used to guarantee the random, but uniform, distribution of points.

In our study the rate of change of the FI with respect to the design variables takes the largest values when $0 \leqslant \beta \leqslant 30$. Consequently, a more dense zone of points is established in this part of the design space (subregion 1, 2, 3 and 4 in Fig. 3). On the other hand, in order to capture the behaviour of the model in the extreme cases, a LHS has been used to distribute points in these specific regions. These points mark the limit of the design space with four "sets" of points, which are distributed in: $(\beta = 0) \wedge (0 \leqslant d \leqslant 47)$, $(\beta = 60) \wedge (0 \leqslant d \leqslant 47)$, $(d = 0) \wedge (0 \leqslant \beta \leqslant 60)$ and $(d = 47) \wedge (0 \leqslant \beta \leqslant 60)$. Finally, a sample of 400 points is created with all these cases (Fig. 3).

[Figure 3 about here.]

3.4. Radial Basis Functions

The RBF [32] interpolation method constructs an approximation function ψ determining the coefficient c_0, c_1 and λ_i to generate a metamodel.

$$\psi = c_0 + c_1 x + \sum_{i=1}^{n} \lambda_i \varphi(\|x - x_i\|) \tag{5}$$

where n is the data sample size, φ is the radial function chosen, x_i is the observed input point and $\|\cdot\|$ is the Euclidean distance. In our case, we can define five different functions: Linear

$\varphi = r$, cubic $\varphi = r^3$, thinplate $\varphi = r^2 \ln(r+1)$, gaussian $\varphi = \exp\left(-\frac{r^2}{2\phi^2}\right)$ and multiquadrics $\varphi = \sqrt{1+\frac{r^2}{\phi^2}}$. Where $r = \|x - x_i\|$ and ϕ is a constant close to the average distance between interpolation points. In addition, smoothing of the values of the RBF in the input points can be carried out to avoid possible input data noise. This smoothing does not force the RBF to obtain a result equal of a specific point of the input data. Thus, the smoothing value acts like the maximum absolute difference between the data point and the approximation provided by RBF. An example of the smoothing is shown in Fig. 4. An optimization with Quasi-Newton method to obtain the optimal smooth values for each radial basis function has been carried out. The smooth value is computed to obtain the minimum RMAE (Section 3.4.2).

[Figure 4 about here.]

In order to reduce the total computational time of the optimization, the FE model has been replaced by the RBF. The automatic parametric model created with *python* and ABAQUS™ generates the "training" sample which is used to construct the RBF. Each model calculated by ABAQUS™ is a input point of the RBF.

3.4.1. Subregion

Sometimes a unique RBF cannot capture the global behaviour of the FE model. For this reason, it is necessary to divide the design space into subregions. Thus, the global RBF has been generated by five smaller RBF.

As a results of a non-linearity observed when $0 \leqslant \beta \leqslant 30$ the design space has been divided in four subregions in that zone. Only one subregion has been created when $30 < \beta \leqslant 60$ as a result of a correct behaviour of RBF in that subregion. It has been checked that the continuity across regions is acceptable. All the different subregions are numbered in Fig. 3.

3.4.2. Accuracy metrics

The accuracy of a metamodel is fundamental to obtain results close to the real case. According to [33, 34] cross-validation error is a common choice to measure the accuracy of the metamodel. In order to compare the different RBFs, a sample of confirmation points is needed. To obtain an

acceptable result comparison, a large sample of confirmation points is generated. LHS is used to distribute 1000 points around the design space which are calculated with the FE model. These design points will be compared with the result of the same point predicted by the RBF. Two performance measures have been used to determine the accuracy of the different RBFs:

(a) Relative average absolute error (RAAE)

$$\text{RAAE} = \frac{\sum_{i=1}^{n} |y_i - \widehat{y}_i|}{n \cdot \text{STD}} \tag{6}$$

(b) Relative maximum absolute error (RMAE)

$$\text{RMAE} = \frac{\max\left(|y_1 - \widehat{y}_1|, |y_2 - \widehat{y}_2|, \ldots, |y_n - \widehat{y}_n|\right)}{\text{STD}} \tag{7}$$

where y_i is the FE value, $\widehat{y}_i$ is the value predicted by the RBF, n is the sample size and STD is the standard deviation of the "training" sample.

RAAE is an indicator of the global accuracy of the RBF. On the other hand, RMAE is more sensitive to error in a specific zone of the design space. Both errors indicate higher accuracy of the metamodel when their results decrease.

3.4.3. Verification of the RBF results

Once the different RBFs have been compared (and selected), a verification of the results obtained is needed. Thus, the sample of confirmation points created to obtain RAAE and RMAE has been used to compute the accuracy of the RBF. The mean of the relative error $\overline{\varepsilon_{\text{r}}}$ and the standard deviation of the relative error $\sigma_{\varepsilon_{\text{r}}}$ have been calculated to achieve a general overview of the accuracy of the RBF.

$$\overline{\varepsilon_{\text{r}}} = \frac{\sum_{i=1}^{n} \varepsilon_{\text{r}}}{n} \quad ; \quad \varepsilon_{\text{r}} = \frac{|y_i - \widehat{y}_i|}{y_i} \tag{8}$$

where ε_{r} is the relative error.

4. Results and Discussion

The error of the subregions has been compared to determine the most accurate function to create the RBF. In our case, a total of ten different radial functions have been compared: the five function described above and their smoothings. RAAE and RMAE have been calculated for each radial basis function and their subregions. The most accurate results have been obtained by using linear smoothing (LS) and multiquadrics smoothing (MS). In an optimization process a reduced value of RMAE is desired, since a large local error in the fitting could lead to a wrong location of the optimal value. According to the results shown in Table 4, LS obtains a 1.07% lower than MS of the mean value of the subregions of RMAE. For this reason, LS has been selected to create the RBF to optimize the run-out.

[Table 4 about here.]

Once the RBF has been chosen the $\overline{\varepsilon_r}$ and σ_{ε_r} have been calculated. The obtained results are listed in Table 5. All the results of $\overline{\varepsilon_r}$ are similar or smaller than 5%. This indicates a correct fit of the RBF and verifies that the RBF is suitable to use in an optimization process. At the same time, it was verified that the RBF and the finite element solution follow the same trend. Results also show that σ_{ε_r} is significant but indicates that 95% of the data (according $\overline{\varepsilon_r} \pm 2\sigma_{\varepsilon_r}$) have an absolute error less than 10%. Also, it is observed that the best results are obtained in subregion 5. This is a new indicator that in this subregion of the design space the variation (or noise) of the data is small and it helps to obtain a RBF more precisely.

[Table 5 about here.]

Regarding computational time, each finite element model created needs about 1 minute considering re-meshing and solution. On the other hand, an evaluation of the RBF is achieved in about 0.005 seconds. Therefore, an optimization with RBF has been finished with about 1 second. Approximately 17 hours would have been required to carry out the optimization with finite element models. The used computer is a HP Compaq dx2400 Microtower with an Intel® Core™ 2 Quad CPU Q8200 with 2.33GHz, 4GB of RAM with Ubuntu 14.04 LTS 64-bits and ABAQUS™

6.12-1 Standard. Quasi-Newton method needed approximately around 60 function evaluations (it depends on the specific interval). On the other hand, the GA needed 51 generations and 1040 function evaluations.

Two different types of problems have been solved. First, those problems in which β needs to be restricted to a short interval of values because of design/manufacturing reason and d may take any value between the global considered bounds (coded as BG). Next, problems in which d has to be restricted because of design/manufacturing reasons and β may take any value between $0°$ and $60°$ (coded as DG). Intervals of $10°$ of β for BG and intervals of 10 mm of d for DG are set (except the last one that is established in 7 mm, DG5 in Table 6). The optimization has been carried out with these different intervals and multiple results of FI have been obtained. Furthermore, the same intervals have been calculated by Quasi-Newton method and GA.

In table 6 the variables and results using Quasi-Newton method (β_{QN}, d_{QN} and FI_{QN}) and GA (β_{GA}, d_{GA} and FI_{GA}) are given. In BG problems, the optimal value of β is always the minimum value of the interval under consideration. Moreover, the optimal value of d_{QN} is always 47 mm (except in the interval BG1 where a value close to 0 is obtained). On the other hand, d_{GA} gets different scattered values in general close to the lower bound of d. This is due to the fact that the objective function depends strongly on β and only slightly on d. Since the GA only performs evaluations of the objective function without computing gradients, the precision of the obtained solution is lower than that achieved with the Quasi-Newton method. With these specific results and observing FI_{GA} of BG we can conclude that the values of FI are similar for $d \simeq 0$ mm or $d = 47$ mm. However, in general, better results are achieved with $d = 47$ mm because we observed that FI_{GA} has a mean of difference of 5.86% higher than FI_{QN}. If DG is analysed we can observe that $\beta_{\text{QN}} = \beta_{\text{GA}} = 0°$ is the result obtained in all the cases for Quasi-Newton method and GAs. This behaviour certifies that the minimum value of β leads to a minimum outcome of FI . On the other hand, for those intervals under consideration where $d < 20$mm (DG1 and DG2), the optimal value of d corresponds to the lower bound of the interval. When considering d between 20 and 30 mm (DG3), the optimal value of d is found at an intermediate point of the interval. Finally, for $d > 30$mm (DG4 and DG5), the optimal value of d is always the upper bound of the interval under consideration. These intervals achieve the minimum result of FI with the maximum value of d .

To understand this behaviour, in Fig. 5 the evolution of B respect to d when $\beta = 0°$ (DG cases) is shown, revealing that from a certain value of d (between 25 and 30 mm) the mixed mode ratio decreases substantially leading to a decrease of the failure index FI . In this moment, a minimum value of FI is obtained with a maximum value of d . In DG only a 0.07% of difference is obtained between the results of FI_{QN} and FI_{GA}.

The global optimum, without intervals, is $\beta = 0°; d = 5.85$ mm and $FI = 4.53$.

[Table 6 about here.]

[Figure 5 about here.]

Both ANOVA and optimization results show that the influence of the β in the results is clear. When $\beta = 0°$ the value of FI is the smallest. This is because the area in the stringer base edge (where the crack appears) decreases as β increases. This part of the stringer base resists and transmits all the tensile stress applied to the panel. For this reason, when this area increases the strength of the interaction panel-stringer increases accordingly. Then, the influence of d is not as significant as that of β .

In the previous work [21], more sophisticated finite element models were carried out. This model was solved in ABAQUS$^{\text{TM}}$ 6.12-1 Standard in which mixed-mode improved cohesive elements [35] were added in the joint between the panel and the stringer to simulate the adhesive. All the results of the present work agree with the results computed in the previous work [21] and the experimental tests carried out by Greenhalgh and Garcia [11]. Both conclude that the stringer run-out with $\beta = 0°$ and $d = 47$ mm is the best design with the highest failure load. Furthermore in [21] it is determined that the second best design is achieved with $\beta = 0°$ and $d = 0$ mm. Therefore, the method used in the present work is reliable since it obtains the same results as experimental tests and finite element models with cohesive elements.

5. Conclusion

A process to design a damage tolerance optimization of composite stringer run-out under tensile load has been presented. A preliminary study of the design variables has been carried out in order

to determine the more influential ones in the opening of the crack between panel and stringer. Metamodelling in terms of Radial Basis Function (RBF) have been used to substitute the results of a finite element model. Moreover, the results of Quasi-Newton method and GA have been compared.

The proposed method involves some trial-and-error process to determine a RBF that properly fits the finite element model results. This process needs of a considerable amount of finite element models. On the contrary, when the RBF is created with an acceptable error, the computational time can be reduces considerably. The authors conclude that the proposed method permits the calculation of a composite material structure with reliability and reduce computational time, discarding some non-influential design variables.

The obtained results show that:

- α and L_{ro} have a very low influence on FI .
- β has an important contribution on FI . On the other hand, d has an influence but it is not relevant enough.
- To obtain better results of FI the lower possible value of β should be used. Regarding d, $d \simeq 0$ mm or $d \simeq 47$ mm could be used. Even though the FI are similar for $d \simeq 0$ mm and $d \simeq 47$ mm, the second ones gives slightly better results when $\beta \neq 0°$.
- When $\beta \simeq 0°$ and $d \simeq 0$ mm the optimum damage tolerance design is obtained.
- RBF is an acceptable metamodeling method which could be useful for similar optimization problems.
- The quality of the initial sampling is vital to create an accurate RBF.
- The optimization of the RBF carried out by Quasi-Newton method is faster and obtains better results than GAs.

Acknowledgments

The authors wish to acknowledge the Ministerio de Economía y Competitividad for the funding of the project MAT2013-46749-R and particularly to Universitat de Girona for the research grant coded as BR2011/02.

References

[1] Vescovini R, Dávila CG, Bisagni C. Failure analysis of composite multi-stringer panels using simplified models. Composites Part B: Engineering 2013;45(1):939–51.

[2] Zimmermann R, Klein H, Kling A. Buckling and postbuckling of stringer stiffened fibre composite curved panels - Tests and computations. Composite Structures 2006;73(2):150–61.

[3] Bertolini J, Castanié B, Barrau JJ, Navarro JP. Multi-level experimental and numerical analysis of composite stiffener debonding. Part 1: Non-specific specimen level. Composite Structures 2009;90(4):381–91.

[4] Bertolini J, Castanié B, Barrau JJ, Navarro JP, Petiot C. Multi-level experimental and numerical analysis of composite stiffener debonding. Part 2: Element and panel level. Composite Structures 2009;90(4):392–403.

[5] Orifici AC, Shah SA, Herszberg I, Kotler A, Weller T. Failure analysis in postbuckled composite T-sections. Composite Structures 2008;86(1-3):146–53.

[6] Meeks C, Greenhalgh E, Falzon BG. Stiffener debonding mechanisms in post-buckled CFRP aerospace panels. Composites Part A: Applied Science and Manufacturing 2005;36(7):934–46.

[7] Orifici AC, Thomson RS, Herszberg I, Weller T, Degenhardt R, Bayandor J. An analysis methodology for failure in postbuckling skin-stiffener interfaces. Composite Structures 2008;86(1-3):186–93.

[8] Faggiani A, Falzon BG. Numerical analysis of stiffener runout sections. Applied Composite Materials 2007;14(2):145–58.

[9] Cosentino E, Weaver PM. Nonlinear analytical approach for preliminary sizing of discrete composite stringer terminations. AIAA Journal 2009;47(3):606–17.

[10] Falzon BG, Hitchings D. The behavior of compressively loaded stiffener runout specimens - Part II: Finite element analysis. Journal of Composite Materials 2003;37(6):481–501.

[11] Greenhalgh E, Garcia MH. Fracture mechanisms and failure processes at stiffener run-outs in polymer matrix composite stiffened elements. Composites Part A: Applied Science and Manufacturing 2004;35(12):1447–58.

[12] Falzon BG, Davies GAO. The behavior of compressively loaded stiffener runout specimens - Part I: Experiments. Journal of Composite Materials 2003;37(5):381–400.

[13] Falzon BG, Davies GAO, Greenhalgh E. Failure of thick-skinned stiffener runout sections loaded in uniaxial compression. Composite Structures 2001;53(2):223–33.

[14] Reinoso J, Blázquez A, Estefani A, París F, Canas J. A composite runout specimen subjected to tension-compression loading conditions: Experimental and global-local finite element analysis. Composite Structures 2013;101(0):274–89.

[15] Psarras S, Pinho ST, Falzon BG. Design of composite stiffener run-outs for damage tolerance. Finite Elements in Analysis and Design 2011;47(8):949–54.

[16] Krueger R, Minguet PJ. Analysis of composite skin-stiffener debond specimens using a shell/3D modeling technique. Composite Structures 2007;81(1):41–59.

[17] Psarras S, Pinho ST, Falzon BG. Investigating the use of compliant webs in the damage-tolerant design of stiffener run-outs. Composites Part B: Engineering 2013;45(1):70–7.

[18] Queipo NV, Haftka RT, Shyy W, Goel T, Vaidyanathan R, Kevin Tucker P. Surrogate-based analysis and optimization. Progress in Aerospace Sciences 2005;41(1):1–28.

[19] Rikards R, Abramovich H, Kalnins K, Auzins J. Surrogate modeling in design optimization of stiffened composite shells. Composite Structures 2006;73(2):244–51.

[20] Jansson N, Wakeman W, Månson JA. Optimization of hybrid thermoplastic composite structures using surrogate models and genetic algorithms. Composite Structures 2007;80(1):21–31.

[21] Badalló P, Trias D, Marín L, Ripoll L. Virtual test of different types of composite stringer run-outs under tensile load; 2015. Under review.

[22] Abaqus 6.12 User's manual. Dassault Systèmes Simulia Corp.; USA; 2012.

[23] Krueger R. The virtual crack closure technique: history, approach and applications. Tech. Rep.; NASA/CR-2002-211628; 2002.

[24] Benzeggagh ML, Kenane M. Measurement of mixed-mode delamination fracture toughness of unidirectional glass/epoxy composites with mixed-mode bending apparatus. Composites Science and Technology 1996;56(4):439–49.

[25] Box GEP, Hunter JS, Hunter WG. Statistics for Experimenters: Design, Innovation, and Discovery. AMC; 2005.

[26] Anderson TL. Fracture Mechanics: Fundamentals and Applications. Taylor & Francis Group; 2005.

[27] Goldberg DE. Genetic Algorithm in search, optimization, and machine learnig. Addison-Wesley publishing company, Inc.; 1989.

[28] MATLAB Optimization Toolbox User's Guide. The Math Works Inc; USA; 2014.

[29] Deb K, Pratap A, Agarwal S, Meyarivan T. A fast and elitist multiobjective genetic algorithm: NSGA-II. IEEE Transactions on Evolutionary Computation 2002;6(2):182–97.

[30] Badalló P, Trias D, Marín L, Mayugo JA. A comparative study of genetic algorithms for the multi-objective optimization of composite stringers under compression loads. Composites Part B: Engineering 2013;47(0):130–6.

[31] Mckay MD, Beckman RJ, Conover WJ. A comparison of three methods for selecting values of input variables in the analysis of output from a computer code. Technometrics 1979;42(1):55–61.

[32] Dyn N, Levin D, Ripa S. Numerical procedures for surface fitting of scattered data by radial functions. Journal Scientific and Statistical Computing 1986;7(2):639–59.

[33] Jin R, Chen W, Simpson TW. Comparative studies of metamodelling techniques under multiple modelling criteria. Structural and Multidisciplinary Optimization 2001;23(1):1–13.

[34] Arian Nik M, Fayazbakhsh K, Pasini D, Lessard L. A comparative study of metamodeling methods for the design optimization of variable stiffness composites. Composite Structures 2014;107:494–501.

[35] Turon A, Camanho PP, Costa J, Renart J. Accurate simulation of delamination growth under mixed-mode loading using cohesive elements: Definition of interlaminar strengths and elastic stiffness. Composite Structures 2010;92(8):1857–64.

[36] Lopes CS, Camanho PP, Gürdal Z, Maimí P, González EV. Low-velocity impact damage on dispersed stacking sequence laminates. part II: Numerical simulations. Composites Science and Technology 2009;69(7-8):937–47.

[37] Renart J, Blanco N, Pajares E, Costa J, Lazcano S, Santacruz G. Side clamped beam (SCB) hinge system for delamination tests in beam-type composite specimens. Composites Science and Technology 2011;71(8):1023–9.

[38] Bonhomme J, Argüelles A, Viña J, Viña I. Fractography and failure mechanisms in static mode I and mode II delamination testing of unidirectional carbon reinforced composites. Polymer Testing 2009;28(6):612–7.

List of Figures

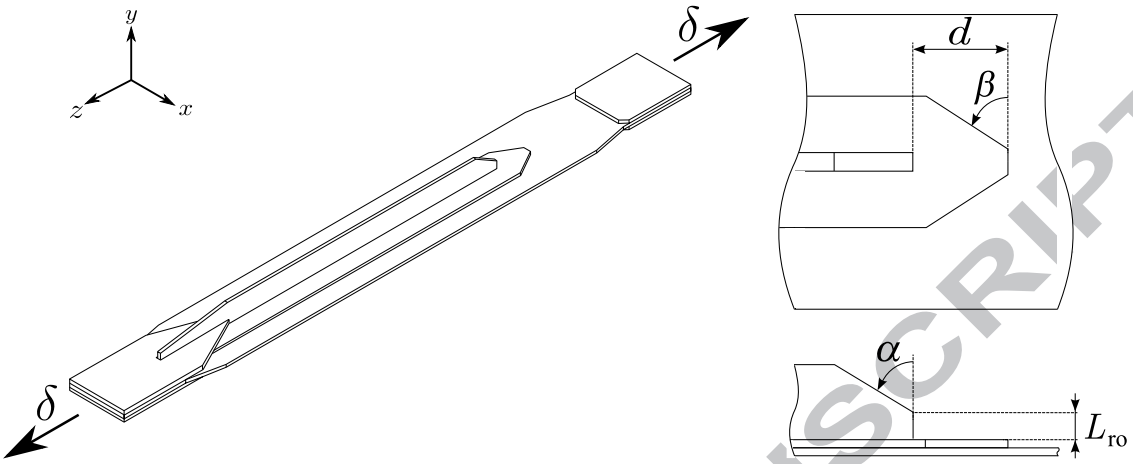

(a) (b)

Figure 1: Schematic representation of the test and the initial design variables.

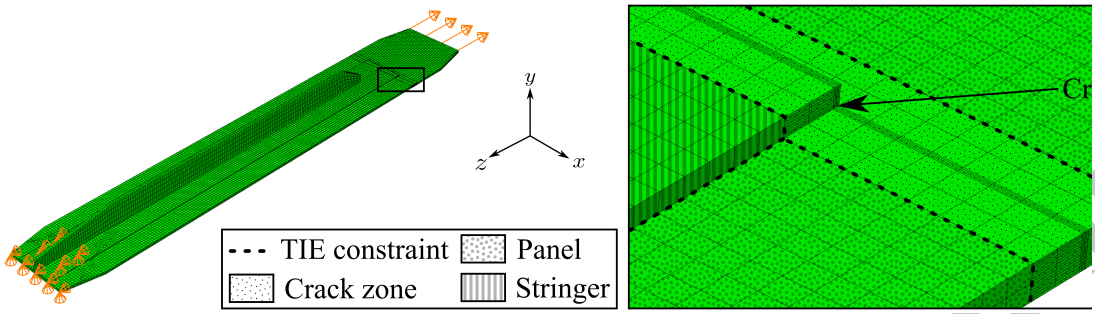

Figure 2: Details of the finite element model.

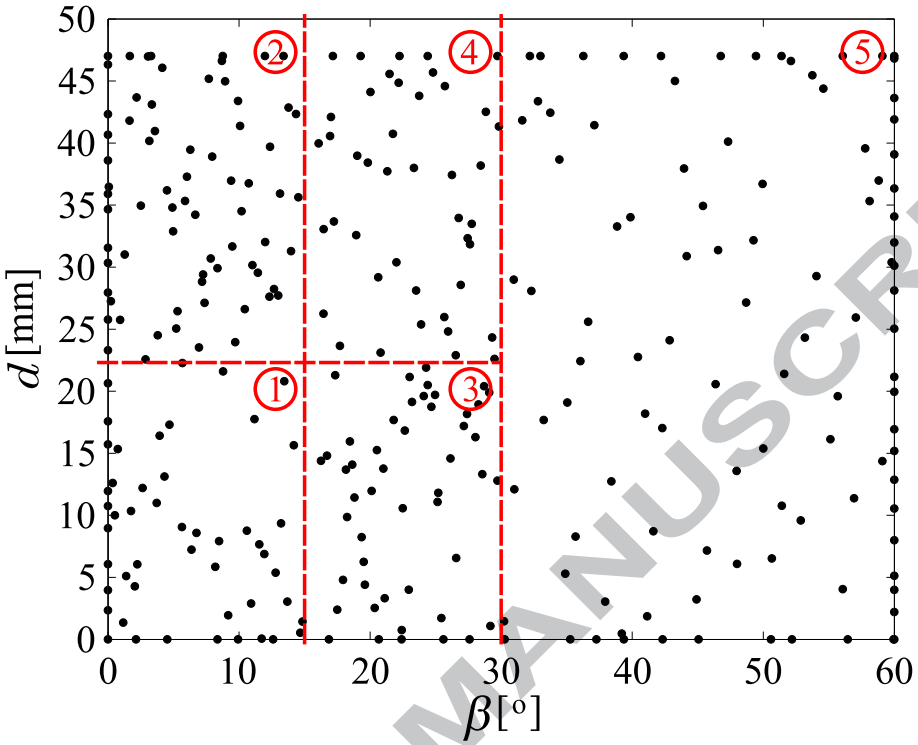

Figure 3: Initial data sampling.

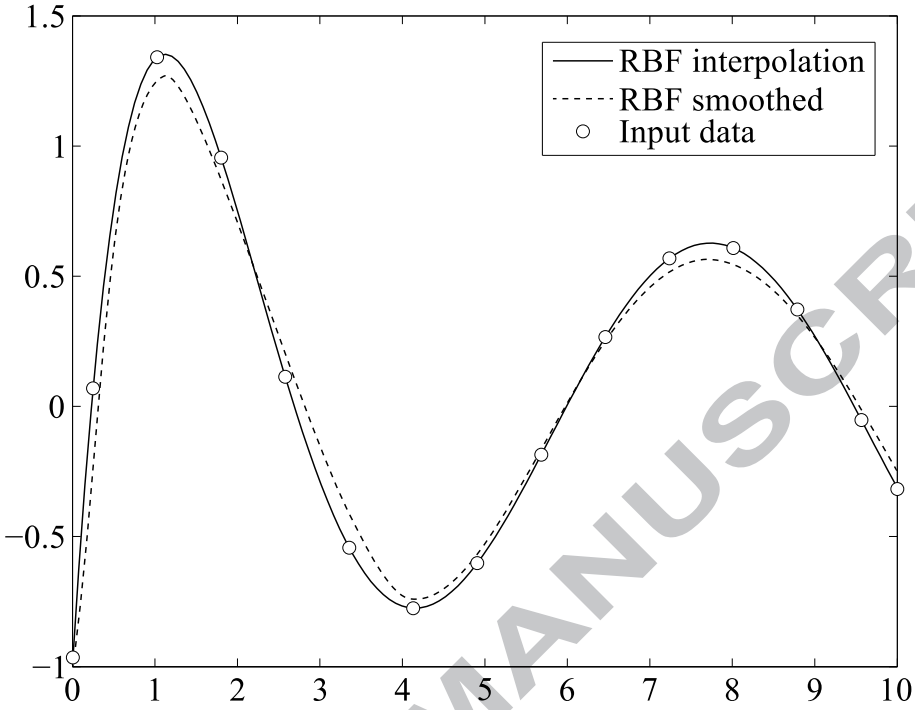

Figure 4: Exemple of smoothed RBF.

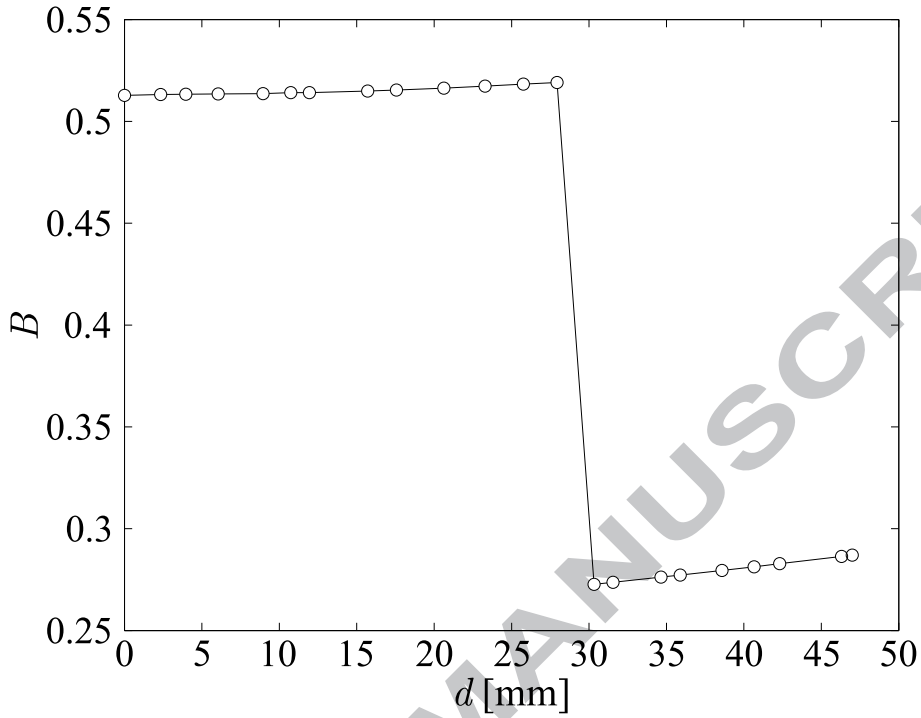

Figure 5: B vs. d when $\beta = 0°$.

List of Tables

Material	Property	Value	Units	Description
AS4/8552*	E_{xx}	135	GPa	Young's modulus in fiber direction.
	E_{yy}	9.6	GPa	Young's modulus in transversal fiber direction.
	E_{zz}	9.6	GPa	Estimated $E_{yy} = E_{zz}$. (transversally isotropic material).
	ν_{xy}	0.32	-	Poisson's modulus in XY plane.
	ν_{xz}	0.32	-	Estimated $\nu_{xy} = \nu_{xz}$. (transversally isotropic material).
	ν_{yz}	0.487	-	Poisson's modulus in YZ plane.
	G_{xy}	5.3	GPa	Shear modulus in XY plane.
	G_{xz}	5.3	GPa	Estimated $G_{xy} = G_{xz}$ (transversally isotropic material).
	G_{yz}	3.228	GPa	Shear modulus in YZ plane.
	X_T	2207	MPa	Longitudinal tensile strength.
	X_C	1531	MPa	Longitudinal compressive strength.
	Y_T	80.7	MPa	Transverse tensile strength.
	Y_C	199.8	MPa	Transverse compressive strength.
	$S_{L_{UD}}$	114.5	MPa	In-plane shear strength.
	$\mathcal{G}_{I_C}$ †	0.2839	N/mm	Critical fracture energy in mode I.
	$\mathcal{G}_{II_C}$ ‡	1.0985	N/mm	Critical fracture energy in mode II.
	ρ	$1.59 \cdot 10^{-9}$	T/mm^3	Density.
FM-300K	$\mathcal{G}_{I_C}$	1.084	N/mm	Critical fracture energy in mode I.
	$\mathcal{G}_{II_C}$	4.931	N/mm	Critical fracture energy in mode II.
	η	6.5687	-	Benzeggagh-Kenane interaction parameter between modes.

* Source: [36]
† Source: [37]
‡ Source: [38]

Table 1: AS4/8552 and FM-300K properties.

Element type	Computation time [s]	Out-of-plane displacement [mm]	Reaction force [N]
C3D8	756	5.569	153 177
C3D8I	1445	5.062	153 629
C3D8R	161	5.694	152 961
C3D20	3402	5.135	153 064
C3D20R	1783	5.135	153 058
SC8R	34	5.048	153 271

Table 2: Results of comparative study of the element type.

Variable	p-value
α	0.6300
β	$2.5351 \cdot 10^{-10}$
d	0.0624
L_{ro}	0.6246

Table 3: Results of the ANOVA test.

Error type	RBF subregion	Linear smoothing	Multiquadrics smoothing
RAAE	1	0.3345	0.3037
	2	0.3650	0.3203
	3	0.6093	0.5803
	4	0.6342	0.6281
	5	0.2444	0.2163
RMAE	1	0.6812	0.6942
	2	0.7420	0.8228
	3	1.4112	1.3642
	4	1.5559	1.6625
	5	1.0094	0.9144

Table 4: Comparative error of RBF.

Linear smoothing		
RBF subregion	$\overline{\varepsilon_r}$ [%]	σ_{ε_r}
1	4.0970	2.2634
2	4.4413	2.5957
3	5.1949	2.6179
4	4.9158	3.0145
5	1.9518	1.8924

Table 5: Results of LS of the RBF.

Code	β interval [°]	d interval [mm]	Quasi-Newton method			Genetic Algorithm		
			β_{QN} [°]	d_{QN} [mm]	FI_{QN}	β_{GA} [°]	d_{GA} [mm]	FI_{GA}
BG1	0-10	0-47	0	5.85	4.53	0	5.85	4.53
BG2	10-20		10	47	7.56	10	2.73	7.69
BG3	20-30		20	47	8.17	20	0.66	8.75
BG4	30-40		30	47	8.51	30	5.87	9.30
BG5	40-50		40	47	9.48	40	4.64	10.29
BG6	50-60		50	47	10.32	50	15.13	10.82
DG1	0-60	0-10	0	5.85	4.53	0	5.85	4.53
DG2		10-20	0	10	5.07	0	10	5.07
DG3		20-30	0	23.5	4.59	0	23.5	4.59
DG4		30-40	0	40	5.54	0	39.37	5.55
DG5		40-47	0	47	5.51	0	45.77	5.52

Table 6: Interval optimums.